Deformation mechanisms of $Al_{0.1}CoCrFeNi$ at elevated temperatures

Tengfei Yang, Zhi Tang, Xie Xie, Robert Carroll, Gongyao Wang, Yugang Wang, Karin A. Dahmen, Peter K. Liaw, Yanwen Zhang

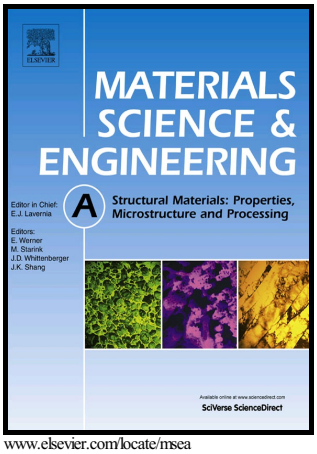

www.elsevier.com/locate/msea

PII: S0921-5093(16)31613-6
DOI: http://dx.doi.org/10.1016/j.msea.2016.12.110
Reference: MSA34541

To appear in: *Materials Science & Engineering A*

Received date: 16 October 2016
Revised date: 10 December 2016
Accepted date: 24 December 2016

Cite this article as: Tengfei Yang, Zhi Tang, Xie Xie, Robert Carroll, Gongyao Wang, Yugang Wang, Karin A. Dahmen, Peter K. Liaw and Yanwen Zhang, Deformation mechanisms of $Al_{0.1}CoCrFeNi$ at elevated temperatures, *Material Science & Engineering A,* http://dx.doi.org/10.1016/j.msea.2016.12.110

Deformation mechanisms of $Al_{0.1}CoCrFeNi$ at elevated temperatures

Tengfei Yang [a,b]*, Zhi Tang [a], Xie Xie [a], Robert Carroll [d], Gongyao Wang [a], Yugang Wang [b], Karin A. Dahmen [d], Peter K. Liaw [a], Yanwen Zhang [c,a]

[a]*Department of Materials Science and Engineering, the University of Tennessee, Knoxville, TN 37996, USA*

[b]*State Key Laboratory of Nuclear Physics and Technology, Center for Applied Physics and Technology, Peking University, Beijing 100871, People's Republic of China*

[c]*Materials Science & Technology Division, Oak Ridge National Laboratory, TN 37831-6138, USA*

[d]*Department of Physics, University of Illinois at Urbana Champaign, 1110 West Green Street, Urbana IL 61801, USA*

Abstract

Deformation mechanisms of a high-entropy alloy with a single face-centered-cubic phase, $Al_{0.1}CoCrFeNi$, at elevated temperatures are studied to explore the high temperature performances of high-entropy alloys. Tensile tests at a strain rate of 10^{-4} s^{-1} are performed at different temperatures ranging from 25 to 700 °C. While both yield strength and ultimate tensile strength decrease with increasing temperature, the maximum elongation to fracture occurred at 500 °C. Transmission electron microscopy characterizations reveal that, at both 25 and 500 °C, most of deformation occurs by dislocation glide on the normal face-centered-cubic slip system, {111}<110>. In contrast, numerous stacking faults are observed at 600

and 700 °C, accompanied by the decreasing of dislocation density, which are attributed to the motion of Shockley partials and the dissociation of dislocations, respectively. According to the Considere's criterion, it is assumed that the dissociation of dislocations and movement of Shockley partials at higher temperatures significantly decreases the work hardening during tensile tests, promoting the early onset of necking instability and decreasing the high-temperature ductility.

Keywords:

High-entropy alloy; Transmission electron microscopy; Mechanical properties; Microstructure

*Corresponding author.

Address: Department of Nuclear Engineering, The University of Tennessee. 100, Estabrook Hall, 1012 Estabrook Road. Knoxville, TN 37996-2300

E-mail address: yangtengfei3745@qq.com (Tengfei Yang).

1. Introduction

High-entropy alloys (HEAs) are multicomponent alloys, which contain at least five major metal elements in a nearly equimolar ratio [1]. Generally, as the amount of the alloying components increases, intermetallic compounds are gradually formed. This trend will cause the difficulty in the microstructure analyses and the inherent brittleness [2]. However, HEAs tend to form simple solid-solution phases, such as face-centered-cubic (FCC) and body-centered-cubic (BCC) phases due to the high mixing entropy [3]. The high mixing entropy can facilitate the formation of disordered solution states and suppress the formation of intermetallic compounds [4]. The simplification of their structures avoids the disadvantages of conventional multicomponent alloys which usually exhibit complicated microstructures and intrinsic brittleness, and the concept of HEAs greatly expands the number of applicable alloy systems.

HEAs have attracted great attention due to their excellent mechanical properties. Based on previous research, it has been found that HEAs can possess high hardness, strong fatigue resistance, good oxidation resistance, and good age-softening resistance. [5-13] Furthermore, Kuznetsov *et al*. [14] studied the microstructures and mechanical properties of the AlCoCrCuFeNi HEA, and found that the forged alloy exhibited superplastic behavior in the temperature range of 800 - 1000 °C. The maximum tensile ductility can reach 860% in the experiment. Bernd Gludovatz *et al*. found that the HEA, CrMnFeCoNi, exhibits a remarkable fracture toughness at cryogenic temperatures, which is attributed to the nanotwinning mechanisms [15].

Much work has been devoted to studying the mechanical properties and microstructures of different HEA systems. However, the deformation mechanisms of HEAs at different temperatures, especially at elevated temperatures, which are of important for understanding their mechanical behavior, have not been fully understood.

The $Al_xCoCrFeNi$ HEA is a well-studied system, and its microstructures and mechanical properties can be well modified by changing the content of Al and fabrication process [11, 16-24]. In the current study, $Al_xCoCrFeNi$ was chosen as a model system for several reasons: (a) its microstructures and mechanical properties have been well-studied; (b) it can form different microstructures as a variation of the Al content, which is convenient for a further systematic investigation; (c) a simple FCC single phase can be formed when the Al content is low ($x < 0.45$), which facilitates the investigation of fundamental mechanisms; and (d) it exhibits good mechanical properties, which make it a very promising system for applications.

In this study, the $Al_{0.1}CoCrFeNi$ HEA was fabricated by vacuum induction-melting and hot isostatic pressing (HIP) sintering. The microstructure of the as-prepared sample was characterized by x-ray diffraction (XRD), scanning electron microscopy (SEM), and transmission electron microscopy (TEM). It was found that only a single FCC phase is formed without nano-precipitates, and the grain size is on the order of millimeter. The hardness was measured using a Vickers hardness tester, and then tensile tests at a strain rate of 10^{-4} s^{-1} were performed at different temperatures ranging from 25 to 700 °C. The microstructures of the HEA samples

tested at different temperatures were characterized by TEM and the serration behavior in the tensile tests was also analyzed. The aim of current study is to investigate the microstructure evolution of HEAs following deformation at different temperatures, which helps understand the plastic-deformation mechanisms of HEAs and opens practical routes for the improvement of mechanical properties.

2. Experimental procedures

The raw elemental materials with at least 99 (weight percent-wt.%) purity were used. Repeated vacuum induction-melting for at least 5 times was carried out to improve the chemical homogeneity of the alloy. The solidified plate was HIP sintering at 1200 °C and 100 MPa for 4 hours. Argon (Ar) gas was used to supply the high pressure. After the HIP sintering, the chamber temperature decreased from 1200 °C to 340 °C in 3 hours, and then decreased to 190 °C in one hour. The prepared sample was cut into small pieces (18 mm×10 mm×1 mm) and polished. The sample used for optical microscopy observation was etched by Kallings reagent.

An XRD (Philips, MRD) was used for the identification of the crystalline structure with the 2θ scan ranging from 20 to 90 °. The SEM and chemical compositions analysis were conducted on a Zeiss LEO1525 equipped with an energy dispersive spectrometry. TEM investigations were conducted in a Zeiss, Libra 200MC operated at 200 kV. The hardness was measured using a Vickers hardness tester under a load of 50 gf for 15 s.

The inset in Fig. 1(a) shows the dimension of the samples used in tensile

experiments. They are tested at a strain rate of 10^{-4} s^{-1} on a MTS810 testing machine at various temperatures, including 25 °C, 500 °C, 600 °C and 700 °C. All of the tensile experiments were conducted in air. For all temperatures above 25 °C, the samples were firstly heated to desired temperatures and then were held there for 15 min before the start of the test. After tensile experiments, thin sheets with a thickness of about 1 mm were carefully cut from gauge sections for the TEM sample preparation. The thin sheets are polished from sides. Therefore, the microstructure was observed along the direction vertical the tensile force in the TEM experiment.

3. Results

Figure 1(a) displays the microstructure of the prepared $Al_{0.1}$CoCrFeNi alloy. Typical dendrite and interdendrite structures were not observed in this material and it only exhibits a single-phase structure with a large grain size (> 1mm). EDS was performed on ten different regions. The average chemical compositions are listed in Table 1. The EDS results indicate that different elements are evenly distributed in the sample, which confirm a single-phase structure, and element concentrations are close to the designed compositions. The effects of grain boundaries are not considered in the deformation processes due to the large grain size.

Figure 1(b) shows the XRD pattern of $Al_{0.1}$CoCrFeNi and identified crystalline structure. Only a FCC structure can be observed, and the corresponding lattice constant is d = 3.57 ± 0.01 Å. This is consistent with previous investigations on the microstructures of Al_xCoCrFeNi, only a FCC structure is found in XRD when the Al

content x is smaller than 0.45 [18, 24].

Figure 2 shows the TEM images and the corresponding selected area electron diffraction (SAED) of the as-prepared $Al_{0.1}CoCrFeNi$. Both images are taken with same zone axis. From the SAED patterns, the zone axis is identified as [110]. No other phase or nano precipitate can be observed on both TEM images. This observation is consistent with the XRD result (Figure 1(b)). Only one grain can be found in the as-prepared TEM sample, indicating the large grain size. TEM images reveal some dislocations [as shown in Fig. 2(a)] and stacking faults [as shown in Fig. 2(b)] present in the HEA sample. These defects may be formed during the high-temperature and pressure process of HIP sintering, but it needs to be further confirmed.

The hardness of the as-prepared $Al_{0.1}CoCrFeNi$ sample in our study is HV 181.3 ± 10. Kao *et al.* [18] measured the hardness of $Al_xCoCrFeNi$ ($0 < x < 2$), and found that the hardness is increased with increasing Al content, which is about HV 120 for $x < 0.3$ (only a single FCC phase is formed) and HV 500 for $x > 0.88$ (only a BCC phase is formed). Another work performed by Wang *et al*. [21] also obtained similar results. The higher hardness of $Al_{0.1}CoCrFeNi$ used in our experiment may be induced by the higher defect density formed in the preparation process. Furthermore, it was found the sample hardness decreases to ~ HV 118 after annealing at 1100 °C for 1 hour.

The engineering stress–strain curves for the $Al_{0.1}CoCrFeNi$ alloy tested at four different temperatures are presented in Fig. 3. The engineering strain is calculated

from the ratio of cross-head displacement to the initial specimen gauge length (28 mm). A distinct yield point followed by a platform region was only observed at room temperature in the current experiment (as shown in the inset of Fig. 3). The discontinuous yielding phenomena may be induced by the dislocation pinning and breakaway from solute atmospheres or short-range order, but the detailed mechanism has not yet been fully clarified [25, 26]. Furthermore, obvious serrations are present on the stress–strain curves of HEA tested at temperatures greater than 25 °C, especially in the large strain region (> 10%), and the extent of work hardening is significantly decreased at 700 °C. It should be noted that the melting point of $Al_{0.1}CoCrFeNi$ is ~1450 °C [23], therefore creep is not considered in the experiment.

Figure 4 shows the evolutions of yield strength, σ_y [0.2% offset, Fig. 4(a)], ultimate tensile strength σ_u [Fig. 4(a)], and elongation to fracture ε_f [Fig. 4(b)] with temperature. The highest tensile yield strength is obtained at room temperature, which is only ~ 300 MPa. This is lower than most of HEAs' yield strength [27], which may be attributed to the single FCC structure and the large grain size. Z. Wu *et al*. studied the mechanical properties of various equiatomic solid solution alloys with face-centered cubic crystal structures, [28] the yield strength of cold rolled FeCoCrNi (grain size ~24 μm) is ~ 290 MPa, which is basically consistent with current study. The difference may be induced by the effects of Al and grain size. Both the yield strength and ultimate tensile strength decrease with increasing temperature, which are essentially consistent with the recent investigation in other HEA systems [28, 29], but the highest value of elongation to fracture is obtained at 500 °C. The elongation to

fracture, ε_f, first increases from 27.25% to 33.73% as the temperature increases from 25 to 500 °C, and then monotonously decreases with increasing temperature. It is worth noting that no significant variation of yield strength, σ_y, was observed between 600 and 700 °C, but the elongation to fracture, ε_f, greatly decreases from 23.04% to 5.85%.

In order to clarify the plastic-deformation mechanisms of $Al_{0.1}CoCrFeNi$ at different temperatures, especially the decrease of elongation to fracture above 500 °C, TEM was performed to observe the defects formed in the tensile deformation. Figure 5 shows the TEM images of the HEA samples tested at different temperatures. The electron beam is somewhat off the crystallographic direction, [110], and $g = (1\bar{1}1)$ is chosen. At 25 °C, a high density of dislocations can be observed and a great amount of dislocations are tangled together, as shown in Fig. 5(a). Due to the high strain (~ 30 %), it is quite difficult to study the dislocation properties, and dislocations with different Burgers vectors can be found by using the $g \cdot b = 0$ technique, indicating that the several slip systems are activated. Further qualitative characterization reveals that the slip of 1/2<110>-type dislocations on <111>-type planes is dominated, as shown in inset of Fig. 5(a). This is consistent with elementary dislocation processes observed in other FCC solid solutions [30, 31]. Figure 5(b) shows the microstructure of the HEA sample tested at 500 °C. Compared with the HEA sample tested at 25 °C, a higher dislocation density can be observed due to the higher strain, and no other defects can be found. This feature suggests that at both 25 and 500 °C, deformation occurs only by dislocation glide.

Figure 5(c) shows the microstructure of the HEA sample tested at 600 °C. Besides the dislocations, some long and narrow straight defects, as indicated by white arrows, can be observed. Electron diffraction reveals that these needle-like defects are located at {111} type planes, similar microstructure is also observed in some other FCC alloys [32, 33]. These defects are identified as stacking faults, the corresponding high resolution image is given in inset. These stacking faults are related with the formation and movement of Shockley partial dislocations, which will be discussed in Sec. 4.2. Figure 5(d) presents the microstructure of the HEA sample tested at 700 °C. The dislocation density is significantly decreased due to the low strain, and two sets of stacking faults can be clearly observed. The interior angle between the two sets of stacking faults is about 70 °, which is in good agreement with the angle of close-packed planes {111} in the FCC unit cell. Furthermore, the morphology of dislocations suggests the dissociation of dislocations occurs, which is also found in some other FCC alloys deformed at high temperatures [29, 33]. It should be noted that no twinning is found in the TEM observation of HEA samples tested at four temperatures.

4. Discussion

4.1 Effect of temperature on yield stress

Generally, the evolution of yield stress versus temperature can be divided into thermal and athermal parts [34]. The thermal part occurs at low temperatures when the thermal activation and atom diffusion is low and dislocation movement is limited

by barriers. As the temperature rises, the dislocation motion is enhanced by thermal fluctuation. Therefore, the yield stress exhibits a significant decrease with increasing temperature in the thermal part region. The athermal part occurs when the temperature is enough high. The increased atomc vibration or random atomic motion at high temperatures facilitates the occurrence of both dislocation sliding and atomic diffusion. Thus the temperature dependence of yield stress in athermal region is weak and the yield stress exhibits a very slow decrease with increasing temperature. [35, 36] The transition between thermal and athermal parts depends on the temperature and atom mobility in the alloy system, and can be determined by the evolution of yield stress versus temperature. For binary FCC alloys, the transition temperature between thermal and athermal regions is often very low, and the athermal region in the yield stress versus temperature curve is large, compared to the thermal region, which is due to the relatively weak barrier strength for dislocation movement. However, the obvious temperature dependence of yield stress can be observed until 600 °C in the current study, as presented in Figs. 3 and 4(a). Similar experimental results are also found in the CrMnFeCoNi and CrFeCoNi HEA, the athermal region does not appear until 1,000 °C [34]. A tentative interpretation is that the shorter distance between different atoms in HEAs, compared to the binary and pure FCC metal, leads to the shorter length scales of obstacles for dislocation movement. This means that a higher temperature is needed to overcome the barrier of dislocation movement [34]. Furthermore, HEAs are composed of different elements with various atom radii, which can cause serious lattice distortion [37]. This trend also can prevent the

dislocation movement. Further investigations about the evolution of yield stress with temperature in different HEAs are needed to clarify the mechanisms.

4.2 The deformation mechanisms of $Al_{0.1}CoCrFeNi$ at different temperatures

Recently, Otto *et al*. [29] studied the influences of temperature and microstructure on the tensile properties of a CoCrFeMnNi high-entropy alloy, which also crystallizes in a single FCC crystal structure. It was found that the yield strength, ultimate tensile strength, and elongation to fracture all increased with decreasing temperature. The TEM characterization indicates that, twinning occurs at a low temperature of 77 K, which provides an additional deformation mode to accommodate plasticity and enhances the ductility. However, no twinning was found in the current study, suggesting that the decrease of elongation to fracture above 500 °C can not be attributed to the twinning behavior.

Figure 6(a) shows the work-hardening degrees (the difference between the ultimate and yield strengths, $\sigma_u - \sigma_y$) and work-hardening rates (derivative of the true stress–strain curves) of $Al_{0.1}CoCrFeNi$ tested at four temperatures. It can be observed that the work-hardening degree during the tensile test is significantly decreased at 600 and 700 °C, which may induce the decrease of elongation to fracture [38, 39]. Furthermore, according to the Considere's criterion, when the work-hardening rate is less than the true stress (A geometric instability region), necking is predicted to occur. As shown in Fig. 6(b), the intersection points between the work-hardening rate curves and the boundary of the geometric instability region (Grey area) indicate the true

stress where necking occurs, and the true stress is basically consistent with the ultimate tensile strength derived from engineering strain-stress curves. For the $Al_{0.1}CoCrFeNi$ alloys tested at 600 and 700 °C, the yield stresses are nearly identical, but the work-hardening rate at 700 °C is much lower than that at 600 °C. This trend suggests that the decrease of elongation to fracture, ε_f, above 500 °C results from the decrease of work hardening.

The TEM characterization shows that many dislocations are formed at 25 and 500 °C, and the deformation occurs only through the dislocation glide. The immovable dislocations and dislocation configurations contribute to the work-hardening during tensile tests [38]. At higher temperatures, the dislocation movement is enhanced, causing the higher work-hardening degree at 500 °C, as shown in Fig. 6(a). Therefore, compared to room temperature, the elongation to fracture, ε_f, is increased at the 500 °C, and the decrease in the ultimate tensile strength is mainly induced by the lower yield stress.

For the temperatures above 500 °C, TEM results reveal that numerous stack faults are formed, as shown in Fig. 5(c). Recently, Zijiao Zhang *et al*. [40] studied the deformation mechanisms of high-entropy alloy CrMnFeCoNi using *in situ* straining in a TEM and also found that a great number of stacking faults on {111} slip planes nucleate and annihilate due to the movement of Shockley partial dislocations is relatively easy in the early stage of deformation. Based on this *in situ* TEM observation, the stack faults in current study are also attributed to the extensive Shockley partial ($\frac{1}{6}$<112> type) dislocation activity. It is assumed that the motion of

Shockley partial dislocations accommodates the strain in the deformation and decreases the dislocation storage, resulting in a low work-hardening. It should be noted that the twinning which also provides an additional deformation mode to accommodate plasticity, can increase the work-hardening and enhance the ductility mainly due to the introduction of twinning boundaries. The twinning boundaries act as barriers of dislocation motion, thus, increasing the work-hardening. In contrast, the barrier effects of stack faults located at slip plane {111} are much weaker than that of twinning boundaries. Therefore, the motion of the Shockley partial dislocations accommodates the strain without significant work-hardening.

At 700 °C, the density of stack faults are increased dramatically, suggesting the movement of numerous Shockley partial dislocations. Furthermore, TEM characterization reveals that the dissociation of perfect dislocations occurs, as shown in Fig. 7(a). The perfect dislocations of $\frac{a}{2}$<110> dissociate into $\frac{a}{6}$<112> Shockley partial dislocations bounding a stacking fault. Figure 7(b) shows the stacking fault fringes, which are the typical characteristic of dissociation of perfect dislocations [33, 41, 42]. The dislocation dissociation significantly decreases dislocation density in the dislocation forests and the barrier strength for dislocation movement, resulting in the decrease of work-hardening. According to Considere's criterion, when the work-hardening rate is smaller than the true stress, necking will occur. The decrease in the work-hardening, therefore, promotes the occurrence of necking, and its ductility is consequently lower.

The differences in the deformation process of different temperatures can be

also observed from the serration morphology in the engineering strain-stress curves. At 500 and 600 °C, oscillations about the general level of the stress-strain curve that occurs in quick succession can be observed, as shown in Fig. 8. According to the classification of the serrated plastic flow, [43] the serration behavior at 500 °C belongs to Type B, which is induced by the discontinuous band propagation arising from the dynamic-strain aging of the dislocation movements within the band. This trend is consistent with the TEM characterization (high density of dislocations can be observed). At 700 °C, some yield drops that occur below the general level of the flow curve can be found. The serration behavior (Type C) is considered to be due to dislocation unlocking and occurs at higher temperatures than in the case of Type B serration. The dislocation unlocking can be interpreted by the dissociation of dislocations. The dislocation density of dislocation forests is decreased, resulting in the dislocations locked by the dislocation forests unlock. Furthermore, we assume that Suzuki segregation may occur at the deformation processes of 700 °C [44]. The occurrence of Suzuki segregation is usually accompanied by the Type C serration [33, 41], of which mechanism is still not clear. Some other characterizations of Suzuki segregation can be also found in current experimental results, such as wide stacking faults, as shown in inset of Fig. 8. In the Suzuki segregation, solute atoms migrate to the dislocations and segregate into the stacking fault bounded by the two Shockley partials, resulting in widening stacking faults, [42] and most of Suzuki segregations are found in binary or ternary concentrated alloys, especially Ni, Co based concentrated alloys [41, 42], due to the high concentration of solute atoms. However,

it is difficult to measure the elemental concentration profiles across both stacking faults and slip bands in the current study to directly confirm the Suzuki segregation [33] due to that there are four major metal elements in the $Al_{0.1}$CoCrFeNi HEA with a nearly equimolar ratio, and the fluctuation of elemental concentration is large.

5. Conclusions

An $Al_{0.1}$CoCrFeNi high-entropy alloy was fabricated by vacuum induction-melting and hot isostatic pressing (HIP) sintering. Only a single FCC phase was formed with a large grain size in the millimeter scale. Tensile experiments at four different temperatures, 25 and 500, 600, 700 °C, were performed. It was found that both yield strength and ultimate tensile strength decrease with increasing temperature, but the highest value of elongation to fracture is obtained at 500 °C. To interpret the mechanical properties, microstructural characterizations were performed after deformation by TEM.

The TEM characterizations revealed that at 25 and 500 °C, deformation occurs mainly by dislocation glide. At higher temperatures, the motion of Shockley partial dislocations provides an additional deformation mechanism to accommodate the strain without significant work hardening, which promotes the occurrence of necking according to the Considere's criterion. Therefore, the highest value of elongation to fracture is obtained at 500 °C. Furthermore, at 700 °C the dissociation of dislocations occurs which further reduces the work hardening and the ductility. The deformation mechanisms derived from TEM characterizations are also consistent with the analysis

of serration behavior in the tensile tests.

Acknowledgements

GY and PKL very much appreciate the financial support from the US National Science Foundation (DMR-0909037, CMMI-0900271, and CMMI-1100080). TY, ZT, and YZ thank the support of the Department of Energy (DOE). Office of Nuclear Energy's Nuclear Energy University Program (NEUP) 00119262. KAD and PKL appreciate the support from DOE, Office of Fossil Energy, National Energy Technology Laboratory (DE-FE-0008855 and DE-FE-0011194). Yugang Wang and Tengfei Yang thank the support of the National Magnetic Confinement Fusion Energy Research Project 2015GB113000, China Postdoctoral Science Foundation 2015M570014 and the National Natural Science Foundation of China (11335003, 91226202).

References:

[1] J.W. Yeh, S.K. Chen, S.J. Lin, J.Y. Gan, T.S. Chin, T.T. Shun, C.H. Tsau, S.Y. Chang, Adv. Eng. Mater., 6 (2004) 299-303.

[2] A. Lindsay Greer, Nature, 366 (1993) 303.

[3] C.-J. Tong, Y.-L. Chen, J.-W. Yeh, S.-J. Lin, S.-K. Chen, T.-T. Shun, C.-H. Tsau, S.-Y. Chang, Metall. Mater. Trans. A, 36 (2005) 881-893.

[4] M.-H. Chuang, M.-H. Tsai, W.-R. Wang, S.-J. Lin, J.-W. Yeh, Acta. Mater., 59 (2011) 6308-6317.

[5] M.A. Hemphill, T. Yuan, G.Y. Wang, J.W. Yeh, C.W. Tsai, A. Chuang, P.K. Liaw, Acta. Mater., 60 (2012) 5723-5734.

[6] C.-Y. Hsu, J.-W. Yeh, S.-K. Chen, T.-T. Shun, Metall. Mater. Trans. A, 35 (2004) 1465-1469.

[7] P.K. Huang, J.W. Yeh, T.T. Shun, S.K. Chen, Adv. Eng. Mater., 6 (2004) 74-78.

[8] J. Chen, L. Lu, K. Lu, Scripta Mater., 54 (2006) 1913-1918.

[9] Y.J. Zhou, Y. Zhang, Y.L. Wang, G.L. Chen, Appl. Phys. Lett., 90 (2007) 181904-181903.

[10] X.F. Wang, Y. Zhang, Y. Qiao, G.L. Chen, Intermetallics, 15 (2007) 357-362.

[11] Y.P. Wang, B.S. Li, M.X. Ren, C. Yang, H.Z. Fu, Mater. Sci. Eng. A, 491 (2008) 154-158.

[12] C.-Y. Hsu, W.-R. Wang, W.-Y. Tang, S.-K. Chen, J.-W. Yeh, Adv. Eng. Mater., 12 (2010) 44-49.

[13] Y.Y. Chen, U.T. Hong, J.W. Yeh, H.C. Shih, Scripta Mater., 54 (2006) 1997-2001.

[14] A.V. Kuznetsov, D.G. Shaysultanov, N.D. Stepanov, G.A. Salishchev, O.N. Senkov, Mater. Sci. Forum, 735 (2013) 146.

[15] B. Gludovatz, A. Hohenwarter, D. Catoor, E.H. Chang, E.P. George, R.O. Ritchie, Science, 345 (2014) 1153-1158.

[16] C. Li, M. Zhao, J.C. Li, Q. Jiang, J. Appl. Phys., 104 (2008) 113504-113506.

[17] C. Li, J.C. Li, M. Zhao, Q. Jiang, J. Alloy Compd., 504S (2010) S515.

[18] Y.-F. Kao, T.-J. Chen, S.-K. Chen, J.-W. Yeh, J. Alloy Compd., 488 (2009) 57-64.

[19] H.-P. Chou, Y.-S. Chang, S.-K. Chen, J.-W. Yeh, Mater. Sci. Eng. B, 163 (2009) 184-189.

[20] A. Manzoni, H. Daoud, R. VÖlkl, U. Glatzel, N. Wanderka, Ultramicroscopy, 132 (2012) 212-215.

[21] W.-R. Wang, W.-L. Wang, S.-C. Wang, Y.-C. Tsai, C.-H. Lai, J.-W. Yeh, Intermetallics, 26 (2012) 44-51.

[22] S.G. Ma, Y. Zhang, Mater. Sci. Eng. A, 532 (2012) 480-486.

[23] C. Zhang, F. Zhang, S. Chen, W. Cao, JOM, 64 (2012) 839-845.

[24] T.-T. Shun, Y.-C. Du, J. Alloy Compd., 479 (2009) 157-160.

[25] R. Ueji, N. Tsuchida, D. Terada, N. Tsuji, Y. Tanaka, A. Takemura, K. Kunishige, Scripta Mater., 59 (2008) 963-966.

[26] N. Tsuji, Y. Ito, Y. Saito, Y. Minamino, Scripta Mater., 47 (2002) 893-899.

[27] C.-W. Tsai, M.-H. Tsai, J.-W. Yeh, C.-C. Yang, J. Alloy Compd., 490 (2010) 160-165.

[28] Z. Wu, H. Bei, G.M. Pharr, E.P. George, Acta. Mater., 81 (2014) 428-441.

[29] F. Otto, A. Dlouhý, C. Somsen, H. Bei, G. Eggeler, E.P. George, Acta. Mater., 61 (2013) 5743-5755.

[30] V. Gerold, H.P. Karnthaler, Acta. Metall, 37 (1989) 2177-2183.

[31] H. Neuhäuser, Acta. Metall, 23 (1975) 455-462.

[32] H. Beladi, I.B. Timokhina, Y. Estrin, J. Kim, B.C. De Cooman, S.K. Kim, Acta. Mater., 59 (2011) 7787-7799.

[33] G.W. Han, I.P. Jones, R.E. Smallman, Acta. Mater., 51 (2003) 2731-2742.

[34] A. Gali, E.P. George, Intermetallics, 39 (2013) 74-78.

[35] T.H. Wille, W. Gieseke, C.H. Schwink, Acta. Metall, 35 (1987) 2679-2693.

[36] T.H. Wille, C.H. Schwink, Acta. Metall, 34 (1986) 1059-1069.

[37] W. Guo, W. Dmowski, J.-Y. Noh, P. Rack, P. Liaw, T. Egami, Metall. Mater. Trans. A, 44 (2013) 1994-1997.

[38] K. Jeong, J.-E. Jin, Y.-S. Jung, S. Kang, Y.-K. Lee, Acta. Mater., 61 (2013) 3399-3410.

[39] O. Bouaziz, N. Guelton, Mater. Sci. Eng. A, 319-321 (2001) 246-249.

[40] Z. Zhang, M.M. Mao, J. Wang, B. Gludovatz, Z. Zhang, S.X. Mao, E.P. George, Q. Yu, R.O. Ritchie, Nat. Commun., 6 (2015).

[41] Y. Koizumi, T. Nukaya, S. Suzuki, S. Kurosu, Y. Li, H. Matsumoto, K. Sato, Y. Tanaka, A. Chiba, Acta. Mater., 60 (2012) 2901-2915.

[42] A. Chiba, M.S. Kim, Materials transactions-JIM, 42 (2001) 2112-2117.

[43] P. Rodriguez, Bulletin of Materials Science, 6 (1984) 653-663.

[44] S. Hideji, Science reports of the Research Institutes, Tohoku University. Ser. A, Physics, chemistry and metallurgy, 4 (1952) 455.

Figures and Figure Captions:

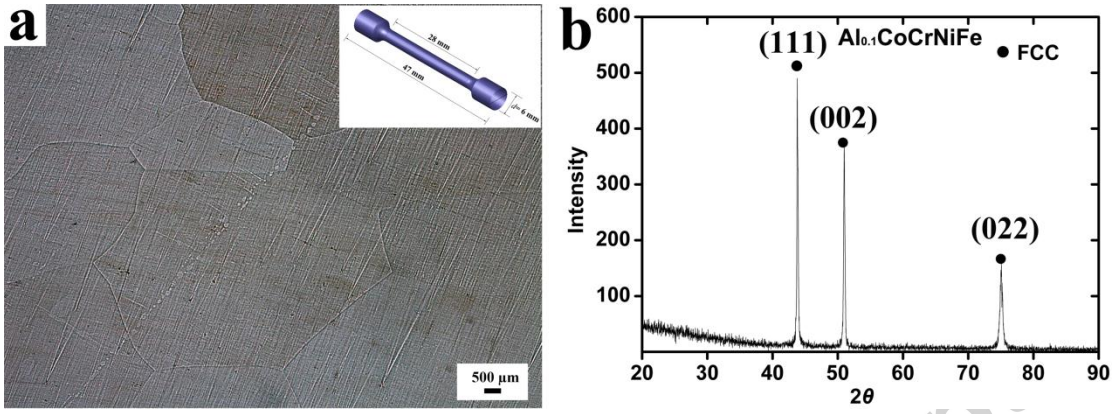

Fig. 1. (a) The optical microscopy image and (b) XRD pattern of the $Al_{0.1}$CoCrFeNi high entropy alloy. The inset shows the dimensions of tensile specimens.

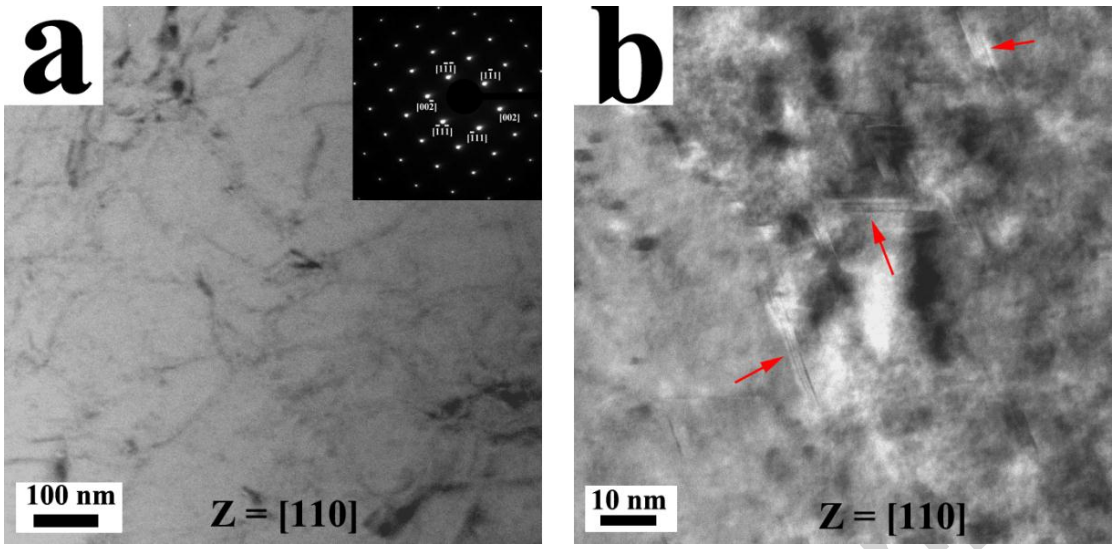

Fig. 2. TEM micrograph and diffraction pattern of as-prepared $Al_{0.1}CoCrFeNi$. The electron beam is along the [110] zone axis. The red arrows in (b) indicate the stack faults.

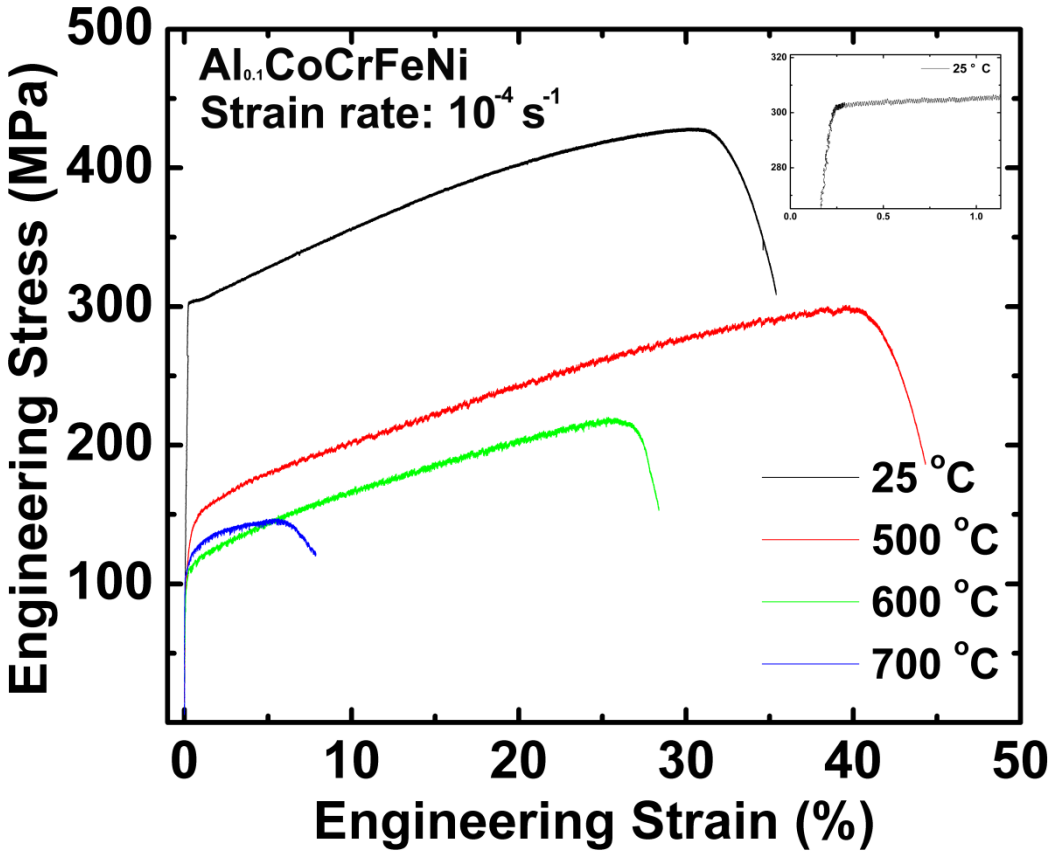

Fig. 3. Engineering stress–strain curves of the $Al_{0.1}$CoCrFeNi alloy at the four testing temperatures. The inset shows the platform region after yielding for the $Al_{0.1}$CoCrFeNi alloy that was tested at 25 °C.

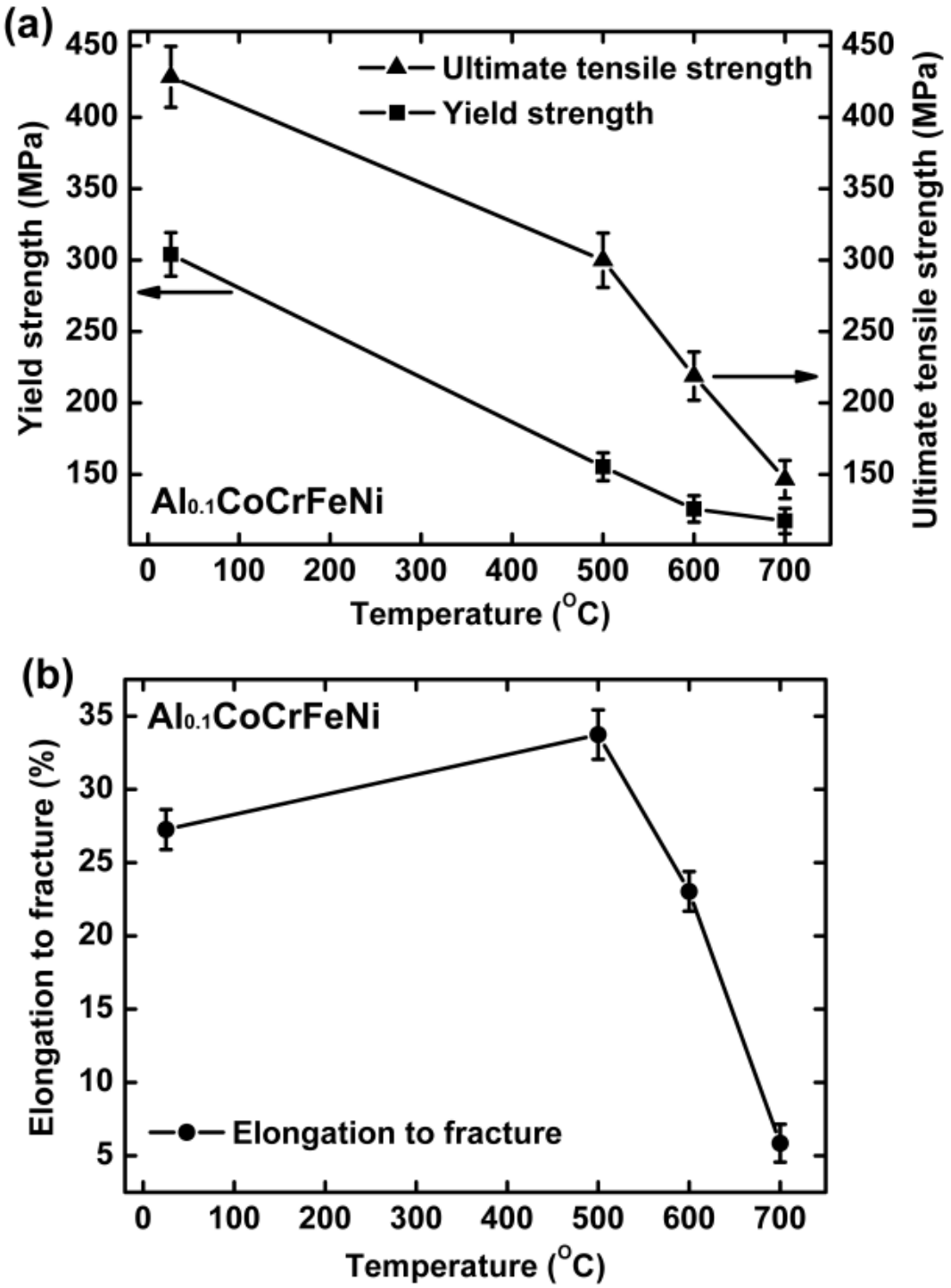

Fig. 4 Temperature dependence of (a) 0.2% offset yield stress, ultimate tensile strength, and (b) elongation to fracture.

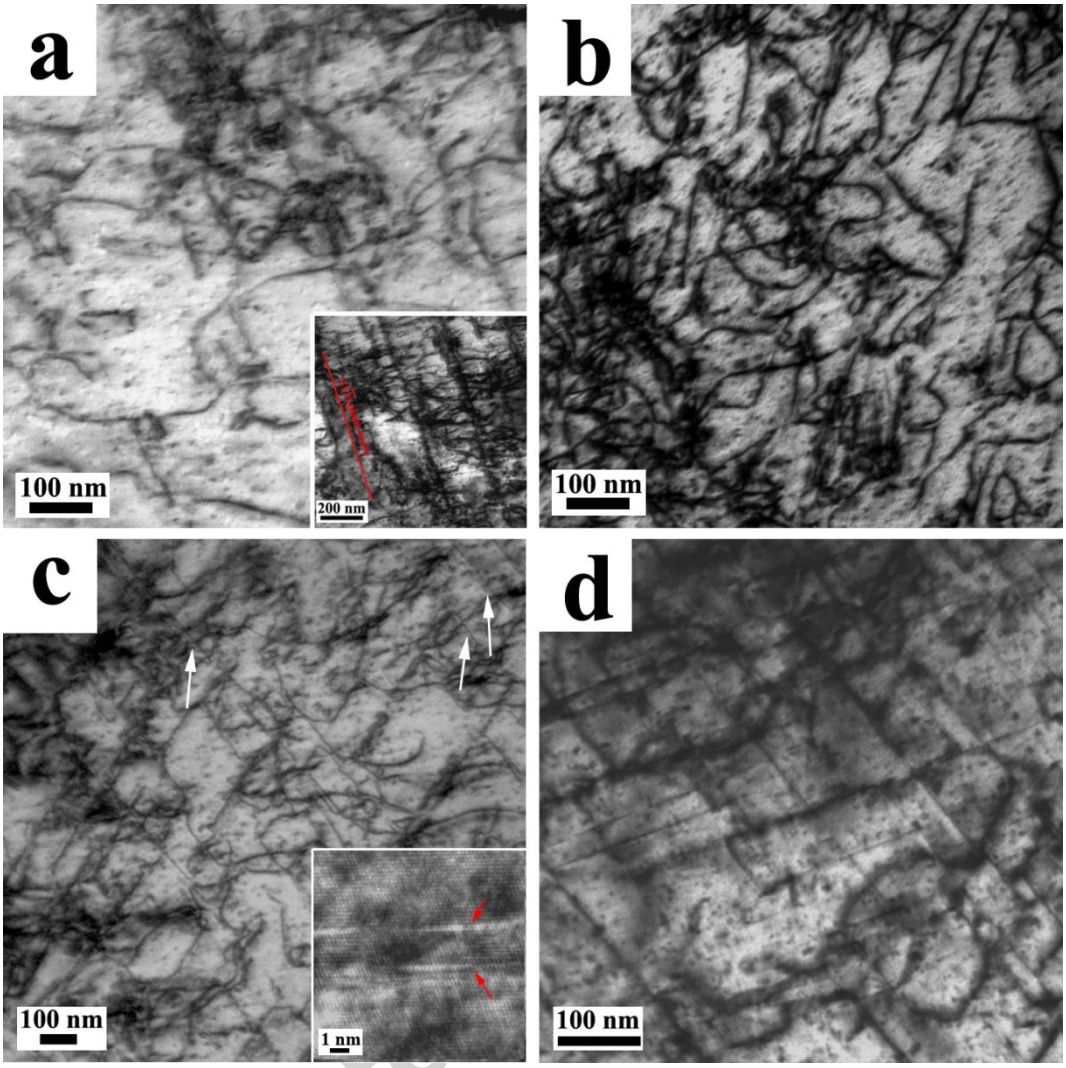

Fig. 5 The microstructures of high entropy alloy, $Al_{0.1}CoCrFeNi$, tested at different temperatures: (a) 25 °C; (b) 500 °C; (c) 600 °C; (d) 700 °C. The inset in (a) shows the {111}-type slip plane. Due to the high strain, several slip systems are activated, and dislocations with different Burgers vectors can be found, but 1/2<110>-type dislocation on {111}-type planes is more than the others. The white arrows in (c) indicate the stacking faults and the inset shows the corresponding high resolution image of stacking faults.

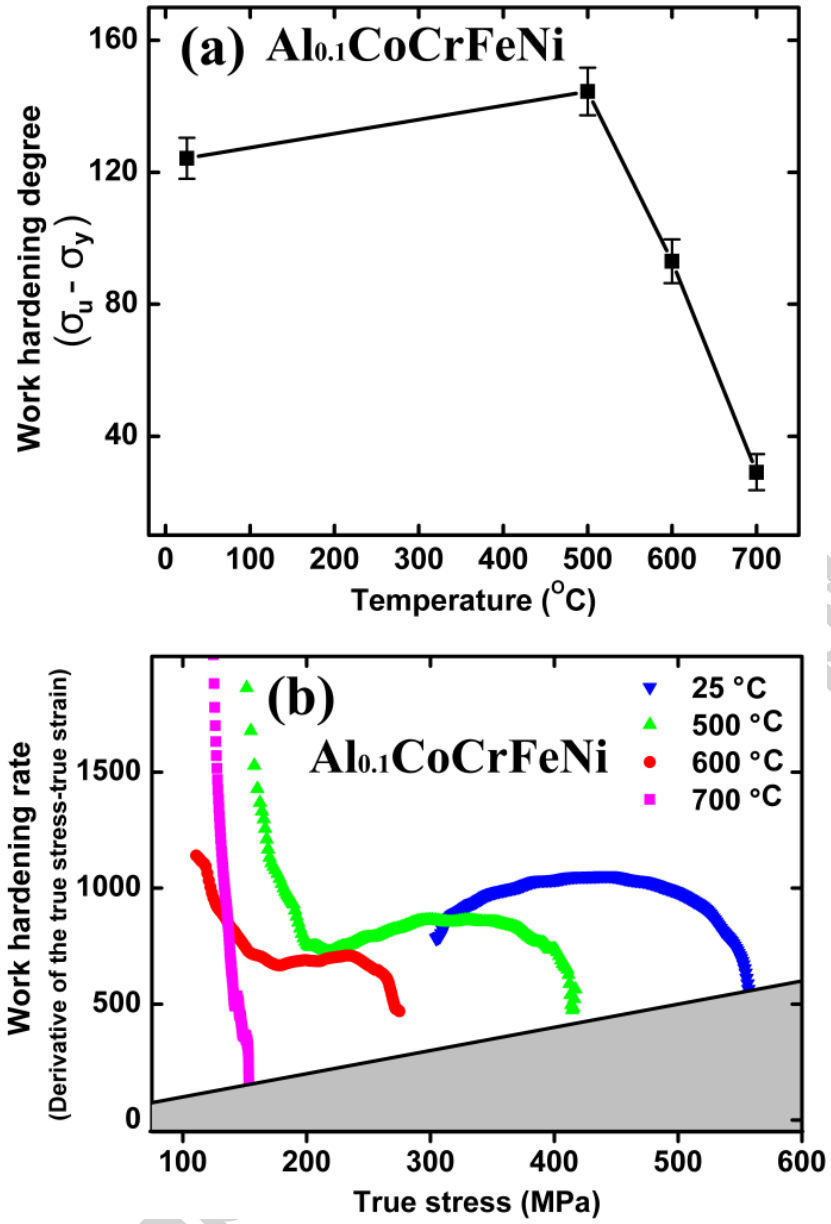

Fig. 6 (a) Temperature dependence of the degree of work hardening in the $Al_{0.1}CoCrFeNi$ alloy (the difference between the ultimate and yield strengths, σ_u-σ_y), (b) Work hardening rate (derivative of the true stress–true strain curves) depicted as a function of the true stress for the $Al_{0.1}CoCrFeNi$ alloy tested at different temperatures. The grey area is the geometric instability region (necking) according to Considere's criterion (the work hardening rate is less than the true stress).

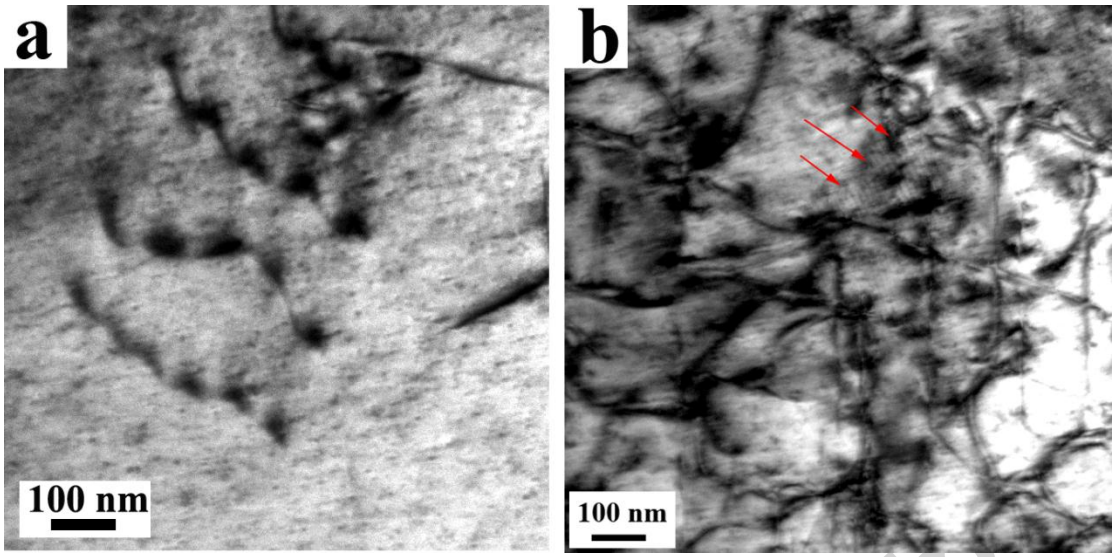

Fig. 7 (a) Dissociated dislocations and (b) stacking fault fringes observed in the $Al_{0.1}CoCrFeNi$ alloy deformed at 700 °C.

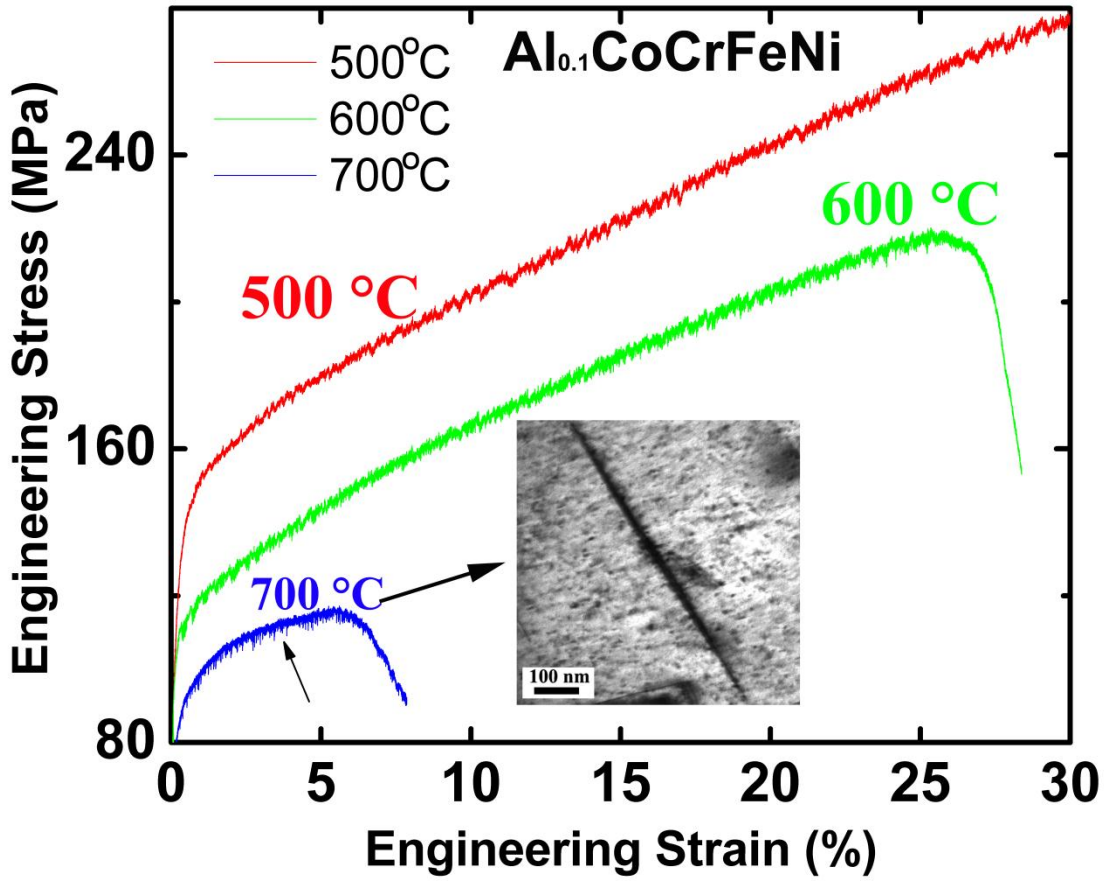

Fig. 8 The engineering stress-strain curves at 500, 600, and 700 °C. The arrows indicate some yield drops that occur below the general level of the flow curve, which are the characterization of Type C serration and cannot be observed at 25 and 500 °C. The inset shows the wide stacking fault formed at 700 °C.

Tab. 1. Chemical composition of as-prepared $Al_{0.1}CoCrFeNi$ alloy

Element (at.%)	Al	Co	Cr	Fe	Ni
	2.2±0.5	24.6 ± 0.5	24.9 ± 0.7	24.2 ± 0.8	24.1 ± 0.8